INTERNATIONAL RESEARCH JOURNAL ON ADVANCED SCIENCE HUB
e-ISSN : 2582 - 4376
Open Access
RSP SCIENCE HUB
(The Hub of Research Ideas)
Available online at www.rspsciencehub.com

Optical and photocatalytic application of $ZnFe_2O_4$–$SmFeO_3$ nanocomposites

*S.K. Rashmi [1], H.S. Bhojya Naik[2,] *, H. Jayadevappa [3]*

[1] *Department of Chemistry, Sahyadri Science College, Shimoga-577203, and Department of Studies and Research in Industrial Chemistry, School of Chemical Sciences, Kuvempu University, Shankaraghatta-577451, Karnataka, India.*

[2] *Department of Studies and Research in Industrial Chemistry, School of Chemical Sciences, Kuvempu University, Shankaraghatta-577451, Karnataka, India.*

[3] *Department of Chemistry, Sahyadri Science College, Shimoga-577203, Karnataka, India.*

rashmisk23dec@gmail.com[1]

Abstract

The $xZnFe_2O_4$–$(1-x)SmFeO_3$ (x = 0.1, 0.2 and 0.3) nanocomposite were synthesised through the thermal decomposition technique and calcinated at 873 K. The obtained nanocomposite was examined using XRD, SEM with EDS, UV-DRS, and TEM with SAED. XRD exhibits a spinel-perovskite mixed structure. The $0.3ZnFe_2O_4$-$0.7SmFeO_3$ nanocomposite showed a substantial red shift in absorption edge with narrow band gap of ~1.8 eV. Further, photodegradation of prepared nanocomposite was assessed for the degradation of Methyl orange (MO). The $0.3ZnFe_2O_4$-$0.7SmFeO_3$ photocatalyst showed effective photodegradation for MO under direct sun light irradiation.

Keywords: Nanocomposite, Spinel, Perovskite, Photocatalyst, Methyl orange

1. Introduction

The contamination of environment with synthetic dyes from industrial wastewater has received increasing attention due to their severe consequences, such as slow biodegradation, aesthetic pollution, toxicity and perturbation to aquatic life [1, 2]. The presence of organic dyes is of major group of water pollutants, may lead to irreversible environmental hazards. To solve these difficulties, more and more research attentions have been focused on development of catalytic materials. With concerns about a clean environment, semiconductor photocatalysis have been the centre of many studies due to their economic and ecologically safe option for solving energy and environment crises [3]. The use of solar energy to eradicate organic pollutants from industrial wastewater makes photocatalysis interesting [4]. Spinel $ZnFe_2O_4$ is a well-known nano-photocatalyst which has been extensively studied due to its narrow band gap and remarkable chemical stability [5]. Nonetheless, the reports on the photodegradation of organic dyes using zinc ferrite as photocatalyst is limited as the activity of pure $ZnFe_2O_4$ is not high enough due to the fast recombination of photogenerated electron–hole pairs [6]. An effective approach to overcome this barrier is to couple $ZnFe_2O_4$ with another semiconductor material since coupling two semiconductors with different energy levels results in mutual transfer of photogenerated electrons and holes from one semiconductor to the other, resulting in an efficient charge separation, an increased life time of the charge carriers, and an

enhanced interfacial charge transfer to adsorbed substrates. Coupling of semiconductors exert the shared benefits of two materials and also accelerate the separation of electron–hole pairs by keeping the reduction and oxidation reactions at two different sites [7, 8].

Xian Ming Liu et al. [9] reported on $CoFe_2O_4$-$BiFeO_3$ nanocomposites and found that this spinel-pervokite system exhibited a strong magnetic property. $REFeO_3$ perovskite-type oxides, rare earth (RE) are very vital materials for composite partner in advanced technologies. $SmFeO_3$ is reported to have a perovskite structure with orthorhombic phases and have been studied extensively as promising photocatalysts [10, 11]. Based on the above facts, in the present paper, we have coupled $ZnFe_2O_4$ with $SmFeO_3$, in the purpose of achieving enhanced photocatalytic activity toward organic dyes.

In this article, spinel-perovskite $xZnFe_2O_4$–$(1-x)SmFeO_3$ (x = 0.1, 0.2 and 0.3) nanocomposites were synthesised by the thermal decomposition technique. The structure of the spinel–perovskite nanocomposites were characterized by means of an X-ray diffractometer and transmission electron microscope. The optical properties of the novel $xZnFe_2O_4$–$(1-x)SmFeO_3$ nanocomposites were studied. These samples were used as photocatalyst in the photodegradation of Methyl Orange.[12-15]

2. Experimental

2.1. Materials

Zinc nitrate ($Zn(NO_3)_2.6H_2O$), iron nitrate ($Fe(NO_3)_3.9H_2O$), samarium chloride ($SmCl_3.6H_2O$), citric acid, ethylene glycol and Methyl Orange (MO) were of analytical grade and used directly as received. Double distilled water was used in the sample preparation.

2.2. Preparation of nano-photocatalyst

The $xZnFe_2O_4$–$(1-x)SmFeO_3$ samples were synthesised by thermal decomposition of precursor gels [10]. The citric acid was added into deionized water with constant stirring and kept at 333K–343 K. Then, ferric nitrate, zinc nitrate and samarium chloride were added in turn. Appropriate molar portions of metal nitrates were fixed at Zn:Sm:Fe ratio of 1:9:11, 1:4:6, and 3:7:13. After the mixing of the salts to their total dissolution, ethylene glycol was added into the solution with a proportion of citric acid to ethylene glycol ratio of 60:40. The temperature was increased up to 363 K. The gels were dried overnight at 373 K in order to remove excess water. During the process of drying, the gel swelled into the fluffy mass and eventually broke into brittle flakes. The samples were grinded and calcinated at 873 K for 4 hours in order to get the oxide materials.

2.3. Analytical and testing instruments

The identification of phase composition and crystalline structure of obtained samples were done by PXRD using PANalytical Xpert Pro X-ray diffractometer with Cu-Kα radiation (λ = 1.5406 Å) in the 2θ range of 10°–80° with a step size of 0.01° and a scan speed of 1 s per step. Transmission electron microscopy (TEM) imaging was performed on a PHILIPS CM 200 microscope operating at 20-200 kV with resolution 2.4 Å. The microstructural morphologies of the $xZnFe_2O_4$–$(1-x)SmFeO_3$ nanocomposites were observed via field emission scanning electron microscopy (FESEM-Carl ZEISS, Supra 40 VP) and chemical composition were examined by energy dispersive X-ray spectroscopy (EDS). The photoabsorption measurement of the $xZnFe_2O_4$–$(1-x)SmFeO_3$ nanocomposite were analysed by UV-Vis spectrophotometer (Shimadzu, UV-1650 PL model) dispersed in ethylene glycol by sonication.

2.4. Photocatalytic experiment

The photocatalytic activities of the $xZnFe_2O_4$–$(1-x)SmFeO_3$ nanocomposites were evaluated by the degradation of Methyl Orange (MO) solution under direct sunlight irradiation. In every experiment, 0.1 g of photocatalyst was added to 100 ml of MO solution (10 ppm). Prior to irradiation, the suspension was magnetically stirred for 30 min in dark to reach the establishment of an adsorption/desorption equilibrium between MO and photocatalyst. Then, at certain time intervals, 5 ml of samples were collected and removed the catalyst particles for subsequent analysis. The change in the concentration (absorbance) of MO solution was

monitored on UV-Vis spectrophotometer by measuring the absorbance in 200–800 nm range using deionised water as reference. Blank tests were also carried out on an aqueous MO solution without photocatalyst under the same condition. In addition, the recyclability of the photocatalyst was also studied by washing and drying the catalyst before the next cycle.

3. Results and Discussion

3.1. Powder X-ray diffraction analysis

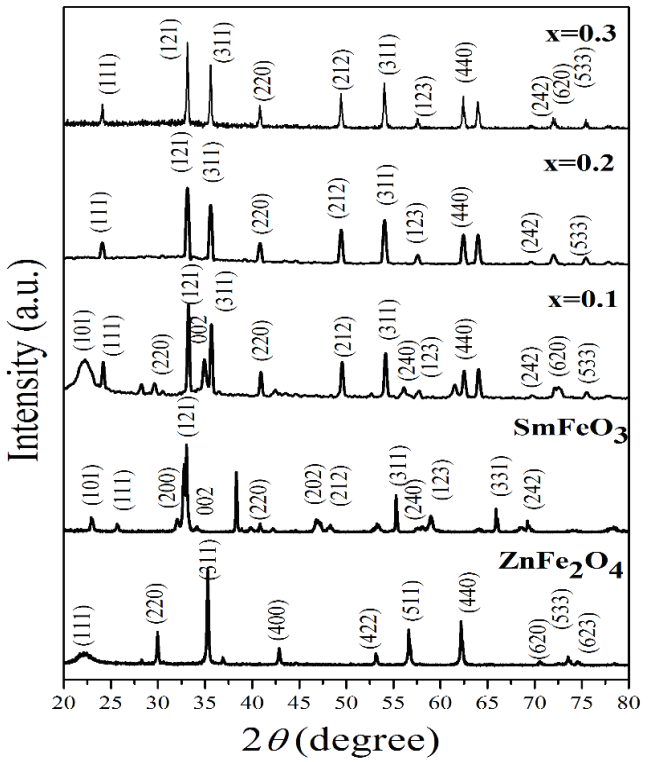

Fig.1. Powder X-ray diffraction pattern of $xZnFe_2O_4$-(1-x)$SmFeO_3$ (x = 0.1, 0.2, 0.3) nanocomposite calcinated at 873 K.

The XRD patterns of the pure $ZnFe_2O_4$, $SmFeO_3$ and $xZnFe_2O_4$–(1−x)$SmFeO_3$ (x = 0.1, 0.2, 0.3) nanocomposite were calcinated at 873 K and are shown in **Fig.1**. The pure zinc ferrite shows strong diffraction peak at 35° which corresponding to the (311) plane of the spinel phase. It was clear that all the diffraction peaks of $ZnFe_2O_4$ can be perfectly indexed as cubic phase with Fd3m (227) space group and match well with the standard card JCPDS card no. 82-1048 (a= 8.442 Å). The $SmFeO_3$ shows the diffraction peak at 33.1° corresponds to the (121) plane of the orthorhombic phase. It was obvious that all the patterns of $SmFeO_3$ express pure perovskite structure, which are accordance with JCPDS card no. 74-1474 (space group = Pbnm(62) a=5.41 Å, b= 5.59 Å, c= 7.71 Å). Furthermore, the distinct diffraction peak displays the formation of the spinel-perovskite mixed structure. The $xZnFe_2O_4$–(1−x)$SmFeO_3$ (x = 0.1, 0.2, 0.3) nanocomposite shows the XRD patterns of $ZnFe_2O_4$ and $SmFeO_3$ which suggest the coexistence of the both $ZnFe_2O_4$ and $SmFeO_3$ in the nanocomposite [12]. The average crystallite size of the $ZnFe_2O_4$, $SmFeO_3$ were calculated using scherrer formula [13] and are 38 and 32 nm, respectively.

3.2. FESEM and EDS analysis

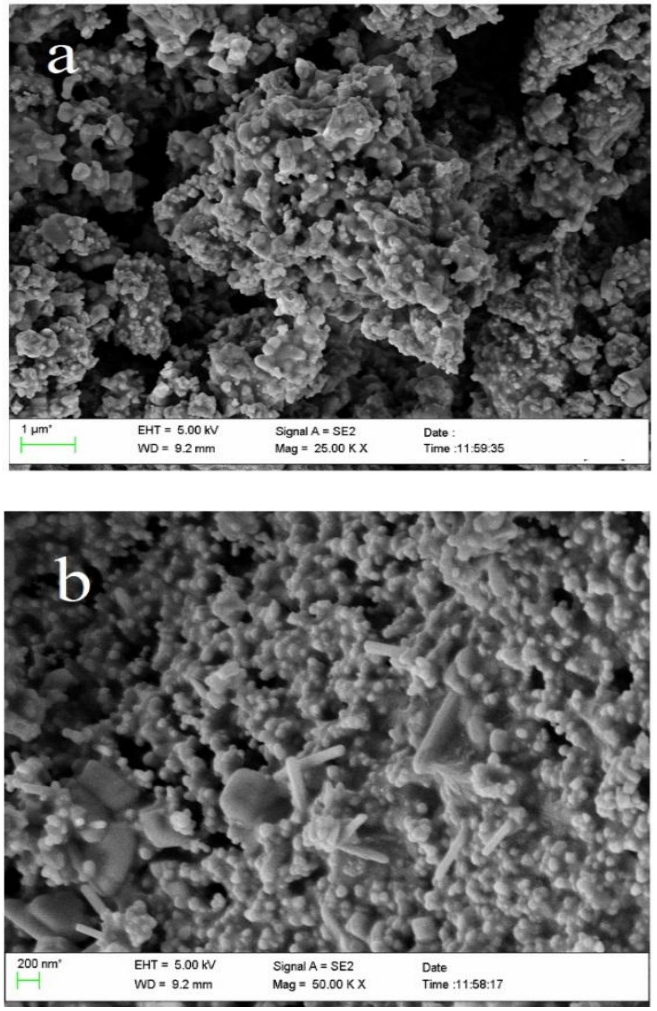

Fig.2. FESEM images of $0.3ZnFe_2O_4$-$0.7SmFeO_3$ nanocomposite calcinated at 873 K.

The morphology of $0.3ZnFe_2O_4$-$0.7SmFeO_3$ sample are shown in **Fig.2a-b**. It was clearly seen that the sample present in irregular shape and most of them are agglomerated. Additionally, the $0.3ZnFe_2O_4$-$0.7SmFeO_3$ nanocomposite is interconnected and fused

together to form open structure and that would be a better for dye adsorption [14-19]. The composition and purity of nanocomposite were investigated using EDS and are shown in **Fig.3**. It indicates the presence of Zn, Sm, Fe, and O atoms as major chemical components in the $0.3ZnFe_2O_4–0.7SmFeO_3$ sample. The atomic ratio of Zn:Sm:Fe were very close to 3:7:13 ratio, which confirms the formation of $0.3ZnFe_2O_4$-$0.9SmFeO_3$ (x=0.3) nanocomposite.

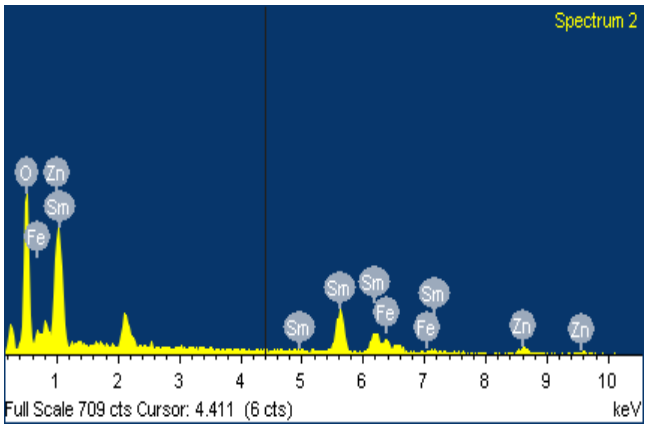

Fig.3. EDS spectra of $0.3ZnFe_2O_4$-$0.7SmFeO_3$ (x=0.3) sample.

3.3. TEM analysis

Fig.4a-b shows TEM images with SAED pattern of $0.3ZnFe_2O_4$-$0.7SmFeO_3$ nanocomposites. It was clear that the particles are in irregular shape and agglomerated to some extent. The selected area electron diffraction patterns of the sample show diffused diffraction spots in circular ring patterns are endorsed to the reflection of spinel $ZnFe_2O_4$ phase and perovskite $SmFeO_3$ phase.

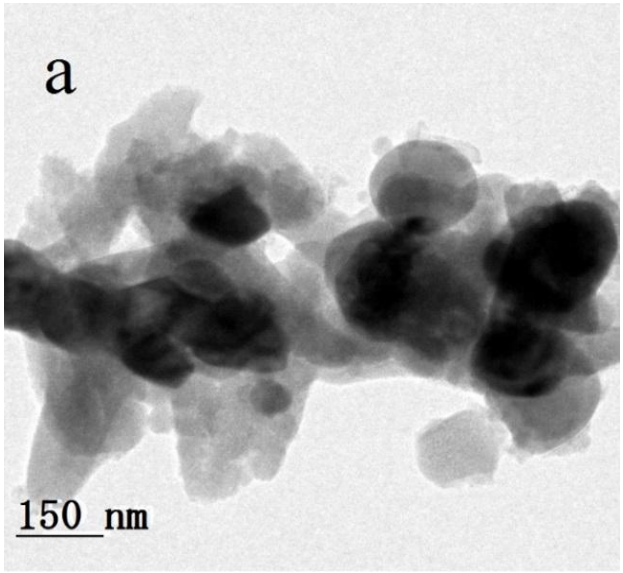

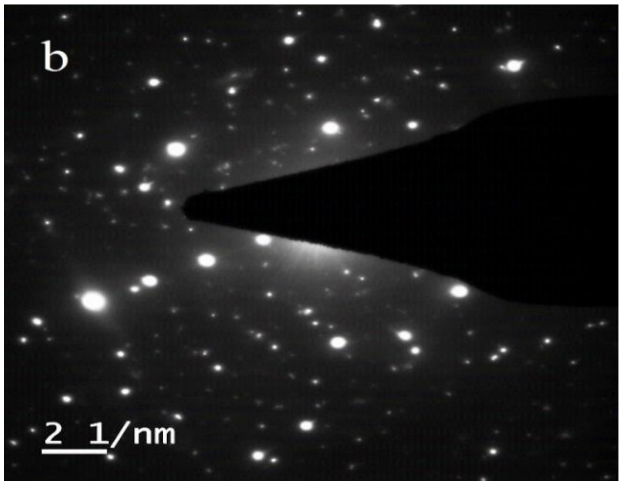

Fig.4. TEM images and selected area diffraction pattern of 0.3 $ZnFe_2O_4$-$0.7SmFeO_3$ nanocomposite.

3.4. Optical properties

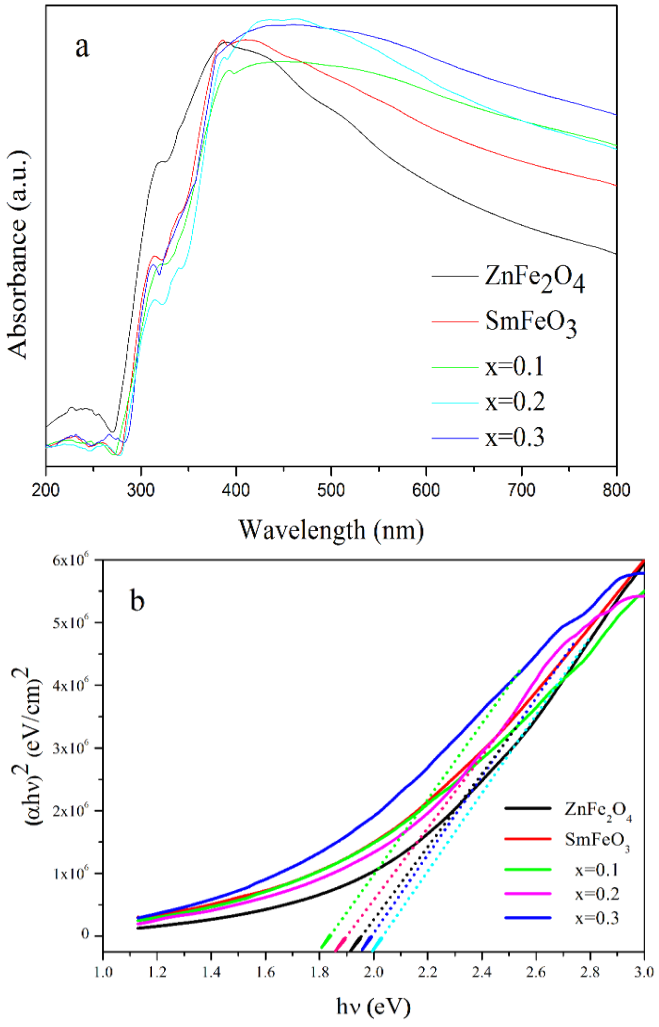

Fig.5.Optical absorption spectra (a) and (b) optical

The Fig.5.Optical absorption spectra(a)and(b) optical band gap from plots of $(\alpha h\nu)^2$ vs. hν to α=0 of $xZnFe_2O_4$-(1-x)$SmFeO_3$ photocatalyst calcinated at 873 K. The optical properties of the $xZnFe_2O_4$–(1−x)$SmFeO_3$ nanocomposites are examined via UV– Vis absorbance spectra. **Fig.5a** shows the absorbance spectra of the pure $ZnFe_2O_4$, $SmFeO_3$, and $xZnFe_2O_4$–(1−x)$SmFeO_3$ composite. The absorption edge of pure $ZnFe_2O_4$, $SmFeO_3$, 0.1$ZnFe_2O_4$-0.9$SmFeO_3$, 0.2$ZnFe_2O_4$-0.8$SmFeO_3$, and 0.3$ZnFe_2O_4$-0.7$SmFeO_3$ samples were 390, 411, 448, 451 and 462 nm respectively. Compared to pure $ZnFe_2O_4$ and $SmFeO_3$, the $xZnFe_2O_4$–(1−x)$SmFeO_3$ samples exhibited strong photoabsorption in visible light region. The absorbance reaches maximum for the 0.3$ZnFe_2O_4$-0.7$SmFeO_3$ sample with x=0.7. Further increase in $SmFeO_3$ concentration (x=0.4) leads to the shifting of absorption curve towards the shorter wavelength (blue shift). From Tauc plot the energy band gap of $xZnFe_2O_4$–(1−x)$SmFeO_3$ nanocomposites were calculated. The band gap energy of all the $xZnFe_2O_4$–(1−x)$SmFeO_3$ samples were calculated from the UV-Vis absorption spectra by plotting the Tauc plot. As shown in **Fig.5b**, the band gap values for pure $ZnFe_2O_4$, $SmFeO_3$, 0.1$ZnFe_2O_4$-0.9$SmFeO_3$, 0.2$ZnFe_2O_4$-0.8$SmFeO_3$, and 0.3$ZnFe_2O_4$-0.7$SmFeO_3$ were 1.95, 1.93, 1.9, 1.86, and 1.8 eV, respectively. The band gap of nanocomposite reduce especially for x=0.3 (0.3$ZnFe_2O_4$-0.7$SmFeO_3$) sample that favoured for the photogenerated charge carriers in photocatalytic process, which inspire us to explore its potential application in heterogeneous photocatalysis under visible light irradiation.

3.5. Photocatalytic performance of 0.3$ZnFe_2O_4$-0.7$SmFeO_3$ nano-photocatalyst

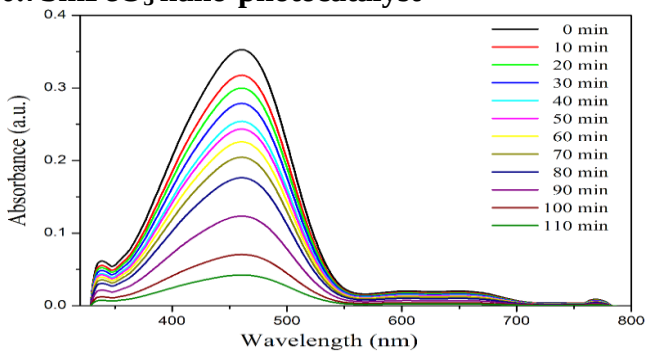

Fig.6. Photodegradation of MO using 0.3$ZnFe_2O_4$-0.7$SmFeO_3$ photocatalyst under solar light irradiation.

Photocatalytic activity of the 0.3$ZnFe_2O_4$-0.7$SmFeO_3$ nanocomposite was evaluated by photodegradation of MO, are shown in **Fig.6**. The MO is a typical anionic dye with a maximum absorption at 463 nm. Blank experiment was performed under same condition without photocatalyst the degradation of MO was negligible. Prior to the photocatalytic reaction, the suspension was stirred to attain adsorption/desorption equilibrium in the presence of photocatalyst without irradiation was achieved (dark reaction). The absorption rates were 11%, which clearly specified that the photocatalyst and sunlight are essential for photodegradations of MO. The suspension was exposed to sunlight irradiation at different interval of time, absorption results were recorded for another 80 min. The gradual decrease in the intensity of MO absorption peak at 463 under solar light irradiation over 0.3$ZnFe_2O_4$-0.7$SmFeO_3$ nanocomposite photocatalyst with the color changing from initial orange to colorless, indicating the photodegradation of MO are shown in **Fig. 6**. The degradation of MO over 0.3$ZnFe_2O_4$-0.7$SmFeO_3$ reaches 91% in 110 min. The greater photodegradation effeciency of 0.3$ZnFe_2O_4$-0.7$SmFeO_3$ sample makes it efficient photocatalyst in the removal of dye. The percentage photodegradation was calculated by following relation.

$$\text{Photodegradation}(\%) = (C_0\text{-}C_t)/C_t * 100 \quad (1)$$

The higher photocatalytic activity of the 0.3$ZnFe_2O_4$-0.7$SmFeO_3$ nanocomposites showed the effective semiconductor coupling, which enhance the photocatalytic activity. The coupling of $ZnFe_2O_4$and $SmFeO_3$, results in an efficient charge separation, an increased lifetime of the charge carriers, and an enhanced interfacial charge transfer to adsorbed substrates [15].

3.6. Mechanism of photocatalytic activity enhancement

The possible mechanism is proposed to explain the enhanced photocatalytic activity of the $xZnFe_2O_4$–(1−x)$SmFeO_3$ nanocomposites, are demonstrated in **Scheme.1**.

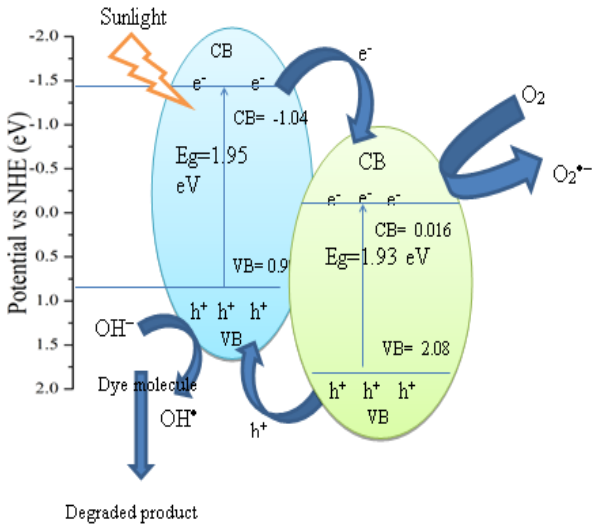

Scheme.1. Possible photocatalytic mechanism of MO degradation over the $xZnFe_2O_4$–$(1-x)SmFeO_3$ nanocomposite under Solar light irradiation

In order to know the separation of photogenerated electron-hole pairs over photocatalytic process. It was necessary to find out the energy level of the $ZnFe_2O_4$ and $SmFeO_3$, their conduction band (CB) and valence band (VB) edge potentials of the components were estimated using the following equations [16, 17]:

$$E_{CB} = \chi - E^e - 0.5E_g \quad (2)$$

$$E_{VB} = E_{CB} - Eg \quad (3)$$

Where χ and Eg denotes the absolute electronegativity and band gap, respectively. E^e is the energy of free electrons on the hydrogen scale (~ 4.5 eV). χ is the electronegativity of semiconductor and it was calculated by the following equation:

$$\chi = [(\chi_A)^a (\chi_B)^b (\chi_C)^c] \quad (4)$$

Where A, B, and C are the different atoms in compound and a, b, and c are number of atoms in the compound [18]. The CB and VB edge potentials of $ZnFe_2O_4$ were calculated as -1.045 and +0.904 eV, respectively. For $SmFeO_3$, CB and VB edge potentials were calculated as +0.0162 and +2.086 eV, respectively. Under solar light irradiation, $ZnFe_2O_4$ and $SmFeO_3$ are excited to produce electron-hole pairs due to its narrow band gap. Subsequently the CB edge of $ZnFe_2O_4$ is more negative than that of $SmFeO_3$, the photogenerated electrons in CB of $ZnFe_2O_4$ easily transfer to the CB of $SmFeO_3$. However, the photogenerated holes on the VB of $SmFeO_3$ migrate to the VB of $ZnFe_2O_4$. As a result, the electrons and holes are increased on the CB and VB of $SmFeO_3$ and $ZnFe_2O_4$, respectively, preventing fast recombination of the charge carriers. These interfacial charge transfers prolong lifetime of the charge carrier by suppressing the recombination of electron-hole pairs, which is more encouraging to enhance the photocatalytic activity of the $xZnFe_2O_4$–$(1-x)SmFeO_3$ nanocomposites, leading to production of more reactive species and has vital role in the degradation reaction. Then, the photogenerated electrons react with adsorbed oxygen and water molecules on the surface of the nanocomposite to produce reactive species of $O_2^{\bullet-}$ and $OH^{\bullet}$ [19]. Meanwhile, the photogenerated holes are trapped by adsorbed H_2O and OH^- to produce $OH^{\bullet}$ species. Therefore, the photocatalytic activity was greatly enhanced in $xZnFe_2O_4$–$(1-x)SmFeO_3$ nanocomposites.

3.7. Recycling of photocatalyst

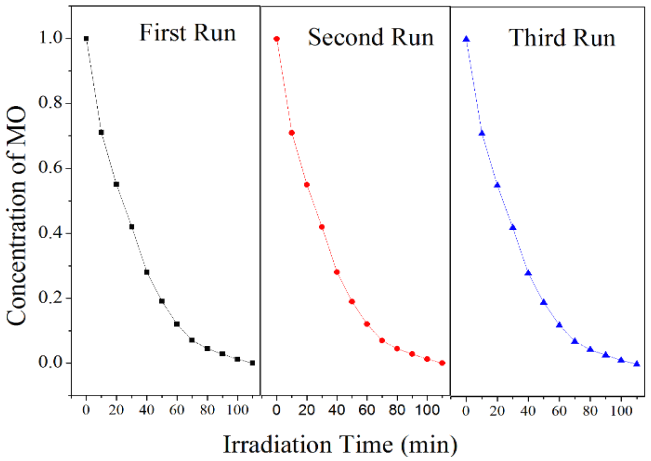

Fig.7. Photocatalytic degradation of MO in three cycles using $0.3ZnFe_2O_4$-$0.7SmFeO_3$ nanocomposite

To probe the regeneration and reusability of the $xZnFe_2O_4$–$(1-x)SmFeO_3$ (x=0.3) nanocomposite for long time performance, MO degradation reactions over this photocatalyst were carried out for three successive runs. In each test, the photocatalyst were gathered by external magnet and reused after washing with water while other factors were kept same. It showed no changes in activity of photodegradation of MO during the three cycles, indicating that the $xZnFe_2O_4$–$(1-x)SmFeO_3$ possessed good stability as photocatalyst. Therefore, it can be concluded that the $xZnFe_2O_4$–$(1-x)SmFeO_3$ was an

outstanding photocatalyst in photodegradation of MO due its reutilization. Further, it could also be used in treatment of wastewaters containing various dye pollutants.

4. Conclusion

In this article, we have reported thermal decomposition technique for synthesis of mixed spinel-perovskite $xZnFe_2O_4$–$(1-x)SmFeO_3$ (x = 0.1, 0.2 and 0.3) nanocomposite. The $0.3ZnFe_2O_4$-$0.7SmFeO_3$ nanocomposite showed a substantial red shift in absorption edge with narrow band gap of ~1.8 eV. The enhanced photocatalytic activity was mainly attributed to the more harvesting ability of visible light and efficient charge separation on the surface of the $xZnFe_2O_4$–$(1-x)SmFeO_3$ nanocomposite. The optimal concentration to achieve the higher photocatalytic activity is x=0.3, due to perfect matching of the band energies for the counterparts. The photodegradation of MO under direct sunlight irradiation was accomplished over $0.3ZnFe_2O_4$-$0.7SmFeO_3$ photocatalyst in 110 min. The nanocomposite displays significant photostability and reusability. Hence it was confirmed that the $0.3ZnFe_2O_4$-$0.7SmFeO_3$ nanocomposite could offer a new solar light induced photocatalyst for further degradation of organic pollutants.

Acknowledgement

One of the authors, S.K. Rashmi expresses their gratitude for University Grant commission (UGC), New Delhi for providing RGNF (JRF-RGNF-2015-17-SC-KAR-12376) and SAIF, IIT Bombay for facilitating HRTEM images.

Reference

[1] Vellaichamy, B., Periakaruppan, P. (2016). Ag nanoshell catalyzed dedying of industrial effluents. RSC advances, 6(38), 31653-31660.

[2] Han, F., Kambala, V. S. R., Srinivasan, M., Rajarathnam, D., Naidu, R. (2009). Tailored titanium dioxide photocatalysts for the degradation of organic dyes in wastewater treatment: a review. Applied Catalysis A: General, 359(1-2), 25-40.

[3] Liyan, W. A. N. G., Hongxia, W., Aijie, W. A. N. G., Min, L. I. U. (2009). Surface modification of a magnetic SiO2 support and immobilization of a nano-TiO2 photocatalyst on it. Chinese Journal of Catalysis, 30(9), 939-944.

[4] Mousavi, M., Habibi-Yangjeh, A. (2016). Magnetically separable ternary g-C3N4/Fe3O4/BiOI nanocomposites: novel visible-light-driven photocatalysts based on graphitic carbon nitride. Journal of colloid and interface science, 465, 83-92.

[5] Li, X., Hou, Y., Zhao, Q., Wang, L. (2011). A general, one-step and template-free synthesis of sphere-like zinc ferrite nanostructures with enhanced photocatalytic activity for dye degradation. Journal of colloid and interface science, 358(1), 102-108.

[6] Valenzuela, M. A., Bosch, P., Jiménez-Becerrill, J., Quiroz, O., Páez, A. I. (2002). Preparation, characterization and photocatalytic activity of ZnO, Fe2O3 and ZnFe2O4. Journal of Photochemistry and photobiology A: Chemistry, 148(1-3), 177-182.

[7] Chiang, Y. J., Lin, C. C. (2013). Photocatalytic decolorization of methylene blue in aqueous solutions using coupled ZnO/SnO2 photocatalysts. Powder technology, 246, 137-143.

[8] Wang, Q., Yu, S., Tan, Z., Zhang, R., Li, Z., Gao, X., Su, H. (2015). Synthesis of monodisperse Bi 2 O 3-modified CeO 2 nanospheres with excellent photocatalytic activity under visible light. CrystEngComm, 17(3), 671-677.

[9] Liu, X. M., Fu, S. Y.,Huang, C. J. (2005). Synthesis and magnetic characterization of novel CoFe2O4–BiFeO3 nanocomposites. Materials Science and Engineering: B, 121(3), 255-260.

[10] Ding, J., Lü, X., Shu, H., Xie, J., Zhang, H. (2010). Microwave-assisted synthesis of perovskite ReFeO3 (Re: La, Sm, Eu, Gd) photocatalyst. Materials Science and Engineering: B, 171(1-3), 31-34.

[11] Niu, X., Li, H., Liu, G. (2005). Preparation, characterization and photocatalytic properties of REFeO3 (RE= Sm, Eu, Gd). Journal of Molecular Catalysis A: Chemical, 232(1-2), 89-93.

[12] Theerthagiri, J., Senthil, R. A., Priya, A., Madhavan, J., Michael, R. J. V., Ashokkumar,

M. (2014). Photocatalytic and photoelectrochemical studies of visible-light active α-Fe 2 O 3–gC 3 N 4 nanocomposites. Rsc Advances, 4(72), 38222-38229.

[13] Moshtaghi, S., Zinatloo-Ajabshir, S., Salavati-Niasari, M. (2016). Preparation and characterization of BaSnO 3 nanostructures via a new simple surfactant-free route. Journal of Materials Science: Materials in Electronics, 27(1), 425-435.

[14] Xin, T., Ma, M., Zhang, H., Gu, J., Wang, S., Liu, M., Zhang, Q. (2014). A facile approach for the synthesis of magnetic separable Fe3O4@ TiO2, core–shell nanocomposites as highly recyclable photocatalysts. Applied Surface Science, 288, 51-59.

[15] Li, W., Feng, C., Dai, S., Yue, J., Hua, F., Hou, H. (2015). Fabrication of sulfur-doped g-C3N4/Au/CdS Z-scheme photocatalyst to improve the photocatalytic performance under visible light. Applied Catalysis B: Environmental, 168, 465-471.

[16] Liu, W., Wang, M., Xu, C., Chen, S. (2012). Facile synthesis of g-C3N4/ZnO composite with enhanced visible light photooxidation and photoreduction properties. Chemical Engineering Journal, 209, 386-393.

[17] Xian, T., Yang, H., Di, L. J., Dai, J. F. (2015). Enhanced photocatalytic activity of BaTiO3@ g-C3N4 for the degradation of methyl orange under simulated sunlight irradiation. Journal of Alloys and Compounds, 622, 1098-1104.

[18] Yuan, Q., Chen, L., Xiong, M., He, J., Luo, S. L., Au, C. T.,Yin, S. F. (2014). Cu2O/BiVO4 heterostructures: synthesis and application in simultaneous photocatalytic oxidation of organic dyes and reduction of Cr (VI) under visible light. Chemical Engineering Journal, 255, 394-402.

[19] Pirhashemi, M., Habibi-Yangjeh, A. (2017). Ultrasonic-assisted preparation of plasmonic ZnO/Ag/Ag2WO4 nanocomposites with high visible-light photocatalytic performance for degradation of organic pollutants. Journal of colloid and interface science, 491, 216-229.